Journal of
Composites Science

MDPI

Article

Optimising Additive Manufacturing to Produce PLA Sandwich Structures by Varying Cell Type and Infill: Effect on Flexural Properties

Gabriele Marabello, Mohamed Chairi and Guido Di Bella *

Department of Engineering, University of Messina, Contrada di Dio, 98166 Messina, Italy; gabriele.marabello@studenti.unime.it (G.M.); mohamed.chairi@unime.it (M.C.)
* Correspondence: guido.dibella@unime.it

Abstract: The objective of this research is to optimize additive manufacturing processes, specifically Fused Filament Fabrication (FFF) techniques, to produce sandwich structures. Mono-material specimens made of polylactic acid (PLA) were produced, where both the skin and core were fabricated in a single print. To optimize the process, variations were made in both the base cell geometry of the core (Tri-Hexagon and Gyroid) and the core infill (5%, 25%, 50%, and 75%), evaluating their effects on static three-point bending behavior. Optical microscopy was employed to assess both the structure generated by additive manufacturing and the fracture modes. The findings reveal that increasing the infill, and thus the core density, enhances the mechanical properties of the structure, although the improvement is such that samples with 50% infill already demonstrate excellent performance. The difference between hexagonal and Gyroid structures is not significant. Based on microscopic analyses, it is believed that the evolution of 3D printers, from open to closed chamber designs, could significantly improve the deposition of the various layers.

Keywords: additive manufacturing; fused filament fabrication; sandwich

Citation: Marabello, G.; Chairi, M.; Di Bella, G. Optimising Additive Manufacturing to Produce PLA Sandwich Structures by Varying Cell Type and Infill: Effect on Flexural Properties. *J. Compos. Sci.* **2024**, *8*, 360. https://doi.org/10.3390/jcs8090360

Academic Editor: Yuan Chen

Received: 17 August 2024
Revised: 5 September 2024
Accepted: 12 September 2024
Published: 14 September 2024

1. Introduction

Additive Manufacturing (AM) [1] plays a crucial role in industrial production [2]. Commonly known as 3D printing, AM enables the creation of complex and innovative structures using innovative materials, depositing layer by layer, and eliminating many of the restrictions associated with traditional manufacturing methods [3]. This manufacturing paradigm represents a significant turning point in design and manufacturing processes [4].

A sandwich panel, also known as a sandwich structure, consists of two strong layers called skins or faces, separated and solidly connected by a central element known as a core. This configuration gives the panel considerable structural stability compared to the individual components. The core, which is usually made of a lightweight, low-strength material, is designed to keep the skins, which are made of high-quality, thin-gauge materials, separate [5,6]. While the skins distribute the loads in the plane, the presence of the core significantly increases the flexural stiffness of the panel, influencing the distance of the faces from the midplane [7]. This concept can be compared to the structure of an I-section beam, where the web contributes to increasing the bending stiffness in the same direction. Increasing the distance between the skins leads to a significant improvement in stiffness without a significant increase in weight. For these reasons, the use of sandwich panels has become increasingly common in the aerospace industry over the past forty years. A common example of a sandwich panel is made of a cardboard material, where the outer layers are flat and separated by a layer of corrugated cardboard. Skins are commonly made from high mechanical strength materials such as fiberglass, carbon or Kevlar composites, or from thin sheets of aluminum or steel. As for the core, structures with honeycomb cells (honeycomb) [8], foams or other materials are used. Honeycomb cells [9] can be

made in several ways, for example by processing thin sheets of aluminum or by forming cells of aramid fibers in a thermosetting resin matrix. However, sandwich panels with honeycomb cores may have some buckling issues. To solve these problems, it is essential to correctly size the cell thickness and cell area. Foams, on the other hand, are cellular materials obtained by dispersing a gas in a solid plastic material. They can be open or closed cell, flexible, semi-rigid or rigid, and made of thermoplastic or thermosetting materials. While foams offer excellent thermal and acoustic insulation, vibration damping, and impact resistance properties, it is important to note that their mechanical properties are inferior to honeycomb cores.

This research aims to explore in depth the advanced potential of additive manufacturing (AM) techniques in the production of sandwich structures, with a particular focus on the creation of complex geometries obtainable exclusively using additive manufacturing. The main objective is to significantly modulate the physical properties of the resulting sandwich structure by intervening on the core geometry, such as the kind of cell, and a process parameter, such as the infill, and keeping the type of material used constant. The material used in this study is polylactic acid (PLA) [10,11].

The intricate structures under study are triply periodic minimal surfaces (TPMS) [12–14], known for their ability to provide lightness and strength. In particular, the investigation focuses on the lightening of the panels through the adoption of these complex geometries [15,16], and on the detailed analysis of their failure behavior. The TPMS surfaces [17], characterized by a continuous configuration without intersections, enable the creation of structures with high mechanical resistance and low mass, ideal for advanced applications.

The TPMS [18–20] geometry under investigation will be compared to a two-dimensional (2D) filling pattern. To achieve these objectives, the research examines in detail the different types of geometries, varying the infill and, consequently, the density of the core. This approach allows us to better understand how these variables influence the mechanical and physical properties of the sandwich panel by optimizing the process of additive manufacturing. Three-point bending tests are carried out to evaluate the performance of the panels with different geometric configurations and filling densities. Three-point bending tests are crucial for determining the mechanical behavior of the panel, offering important data on the failure behavior of the panels.

The ultimate goal is to develop sandwich panels with optimal physical properties for specific applications [21], using additive manufacturing to overcome the limitations of traditional production techniques [22]. These panels could find application in sectors such as aerospace, automotive and biomedical [23], where the combination of lightness and resistance is particularly advantageous [24].

This study aims to analyze complex geometries for the creation of the core of sandwich structures [25], focusing on geometries not yet used in the production of such panels [26,27]. In particular, we chose to examine a 2D structure, derived from the honeycomb structure [28], known as “Tri-Hexagonal”, and a 3D structure, i.e., formed by an elementary cell that repeats itself unchanged in the three directions of space [29], in order to evaluate the impact of the third dimension on the repeatability of the elementary cells [30]. In this specific case, a structure known as a triply periodic minimal surface (TPMS), or a “Gyroid”, selected for its intrinsic physical properties, will be analyzed. The 2D structure, characterized by hexagons connected by triangles, offers high stability in the X and Y directions and moderate stability in the Z direction.

This study introduces an innovative approach to optimizing the mechanical properties of 3D-printed PLA sandwich structures by exploring both traditional (Tri-Hexagon) and novel (Gyroid) cell geometries. By systematically varying the infill density, the research offers new insights into how these geometric configurations can be fine-tuned to achieve specific performance goals. The ability to manipulate these parameters through additive manufacturing represents a significant advancement over conventional manufacturing methods, which are often limited in their capacity to produce complex, customized structures with such precision.

Among the main developments that this research activity can have, there are both design and production evolutions. It is plausible to hypothesize that the use and testing of other types of filling, be they two-dimensional or three-dimensional geometries, could enrich the literature with significant examples of the application of additive manufacturing in the field of sandwich structures. The testing of lattice geometries, known as "lattice structures" [31], which are easily achievable using AM, is also envisaged. Furthermore, the possible change in technology must be considered, moving from the current FDM used in this work, to other types of additive manufacturing [32], which could broaden the horizons of this research. Finally, the production of specimens via multi-material FDM printing is planned, with the aim of creating composite sandwich structures in which it will be possible to use different materials [33], both for the skins and for the core of the panel, including composite materials containing polymers [34] and fibers [35–37], short or long, made of materials such as carbon [38,39], Kevlar or vegetable fibers [40–42].

2. Materials and Methods

In the present work, innovative sandwich panel specimens were generated and produced using additive manufacturing techniques with consequent mechanical characterization through three-point bending tests. The core of these sandwich structures was modeled with the help of two different types of geometries: Tri-Hexagonal (2D) and Gyroid (3D). These geometries, or patterns, were generated with four different filling percentages: 5%, 25%, 50%, and 75%. The filling percentage, in the merit of additive manufacturing technologies [43], is also defined through the term "infill". This parameter indicates the percentage of fullness present inside the component in relation to the void, meaning that an infill equal to 0% indicates an empty component while 100% filling indicates a completely full component.

The research methodology follows established standards to ensure consistency and reliability. Specifically, the flexural tests were conducted in accordance with the ASTM D790 standard, which outlines the procedures for testing the flexural properties of plastics. The optimization process was structured around this standard, with the objective function being the maximization of flexural strength relative to the material used. Constraints included the selected infill densities and cell geometries, which were chosen based on their relevance to real-world applications. This adherence to standard testing protocols ensures that the findings can be compared with other studies and applied in practical scenarios.

In the next sections, the design and manufacturing process will be discussed, with particular attention to the geometries used and the related geometric parameters, such as their filling density.

2.1. Design of Specimens

We proceeded by examining the process of producing the specimens; specifically, it is noted that additive manufacturing technologies are based on a process known as "design-driven manufacturing". The procedure begins with the three-dimensional design of the component using three-dimensional design software, such as CAD version 24.2 (Computer Aided Design). In the context of this study, parametric modeling was performed using Autodesk Inventor software 2022. For the creation of the specimens, reference was made to the D790 standard, through which the appropriate dimensions with which to create the specimens were chosen; finally, the specimens were weighed, and the relative weights were reported in Table 1. The dimensions of the bending test specimens are 122.9 mm × 25.5 mm × 6.4 mm. It is evident that the difference in weight between the two cells is low.

Table 1. Mean weight of each kind of sample.

	5%	25%	50%	75%
Trihexagonal	8.32 g	11.87 g	15.93 g	19.91 g
Gyroid	8.47 g	11.96 g	16.06 g	20.21 g
	+1.80%	+0.75%	+0.82%	+1.51%

Once the CAD modeling was complete, the file was exported in a format called STL (Stereo Lithography Interface Format). This format represents a solid whose surface is discretized into triangles. Essentially, the STL file contains the X, Y, and Z coordinates for each of the three vertices of each triangle, along with a vector describing the orientation of the surface normal of the triangle in question. The STL file was imported into the slicing software. A slicing software is an application used mainly in the field of 3D printing. This type of software is designed to convert digital 3D models into specific instructions, called "slices", that a 3D printer can understand and use to create a physical object layer by layer. The slicing process involves dividing the 3D model into a series of thin horizontal layers, determining the paths that the printer will take to deposit the material and create each layer. This software allows the customization of various printing parameters, such as infill density, print speed, and other settings, to achieve optimal results based on your specific project needs. Some examples of slicing software include Cura, Simplify3D 3.1.0, Slic3r 1.3.0, and PrusaSlicer 2.8.0. UltiMaker Cura software version 5.7.2 was used in this study. Within this software it was possible to modify the cell configuration and the infill. For the purposes of this study, two different types of filling configuration were taken into consideration:

- The Tri-Hexagon pattern (Figure 1a) is a distinctive geometric pattern used in 3D printing and various engineering applications due to its excellent mechanical characteristics. Geometrically, this pattern combines regular hexagons with equilateral triangles that fill the spaces between the hexagons. Regular hexagons are six-sided polygons with internal angles of 120 degrees, and in a two-dimensional grid, each hexagon is surrounded by other hexagons, creating a tessellated arrangement with no gaps. Between each pair of adjacent hexagons, there are equilateral triangles, all of which have three equal sides and internal angles of 60 degrees. Each equilateral triangle fits perfectly into the spaces between three adjacent hexagons. The combination of hexagons and triangles creates a periodic structure that repeats itself infinitely in all directions of the plane, giving the pattern a high degree of geometric symmetry. The Tri-Hexagon pattern can be visualized as a mesh whose nodes are the vertices of the hexagons and triangles, contributing to the uniform distribution of the applied forces across the structure. The combination of hexagons and triangles creates a network that evenly distributes the mechanical forces. The hexagons provide stability and compressive strength, while the triangles reinforce the structure and prevent deformation. Hexagons, known to be one of the most efficient shapes for stress distribution, together with triangles, contribute to high stiffness, which is essential to resist deformation under load. The Tri-Hexagon pattern enables efficient use of material and reduces the overall mass of the structure without compromising strength. This is particularly useful in 3D printing where the aim is to reduce weight while maintaining mechanical properties. The geometric configuration of the Tri-Hexagon pattern takes advantage of the optimal arrangement of hexagons and triangles to maximize mechanical properties, giving a unique combination of lightness, strength and stiffness, ideal for advanced applications in 3D printing and engineering. Its excellent mechanical characteristics arise from the ability to evenly distribute forces and use the material efficiently, making it a preferred choice for structures requiring a balance between strength and lightness.
- The TPMS (Triply Periodic Minimal Surface) [44–46] Gyroid structure (Figure 1b) is an advanced geometric model used in 3D printing and various fields of engineering due to its extraordinary mechanical and physical properties. Geometrically, a Gyroid surface is one of the minimal triply periodic surfaces, characterized by a continuous

and intersection-free configuration that repeats three-dimensionally in space [47]. This surface is mathematically defined and has a constant mean curvature of zero, meaning that every point on the surface is subjected to uniformly distributed tensile forces. The Gyroid is composed of a network of sinusoidal channels [48] that intertwine in three spatial directions and form a highly symmetric and periodic structure. The complexity of the Gyroid lies in its ability to divide space into two interconnected but non-overlapping regions [49,50], creating a three-dimensional lattice [51,52] that offers high mechanical resistance and great lightness. This configuration allows a uniform distribution of forces across the entire structure and makes it particularly resistant to both compression and tension. The Gyroid configuration maximizes the strength-to-weight ratio through efficient material distribution. This geometric model allows you to create components with an optimized internal structure, reducing the amount of material needed without compromising overall strength [53]. The Gyroid surface is particularly effective at absorbing and dispersing energy [54,55], making it ideal for applications requiring high shock absorption and superior mechanical strength. In 3D printing, the Gyroid structure is used as an infill to improve the mechanical properties [56,57] of the printed objects. Thanks to its unique geometric configuration, the Gyroid offers an optimal balance between rigidity and flexibility, making it suitable for a wide range of applications, from aerospace to biomedical. 3D printing allows the fabrication of Gyroid structures with a high degree of precision, fully exploiting the potential of this minimal surface to create advanced components with superior mechanical and physical properties. Like some other triply periodic minimal surfaces, the Gyroid surface can be approximated trigonometrically by a short equation (Equation (1)):

$$\sin x \cdot \cos y + \sin y \cdot \cos z + \sin z \cdot \cos x = 0, \quad (1)$$

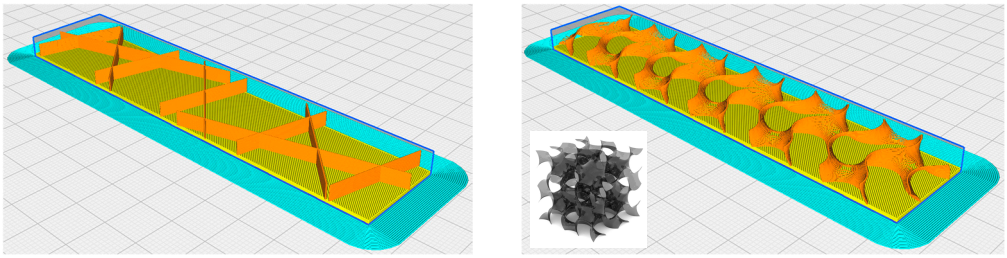

(**a**) (**b**)

Figure 1. Filling configurations (examples with 5% infill): (**a**) Tri-Hexagon pattern; (**b**) TPMS (Triply Periodic Minimal Surface) Gyroid structure.

After slicing the model in the appropriate software, the file is transferred to the 3D printer, which then creates the component using the various additive manufacturing technologies available. The test specimen is positioned on the printing surface so that the smallest dimension, i.e., the thickness, aligned along the Z-axis of the machine, and the horizontal layers at a 90° to the testing machine [58,59]. After production, the manufactured component can be subjected to post-production treatments, if necessary, which may include chemical and thermal treatments as well as finishing processes using machine tools. In the subject of this study, no post-production treatments were implemented.

2.2. Production of Specimens Using Additive Manufacturing Techniques

In this study, the additive manufacturing technology called "Fused Deposition Modeling" (FDM) [60] was used, with an "Artillery Sidewinder X2" 3D printer. Table 2 shows the data relating to the printing parameters of the specimens [61] and the photo of the 3D printer.

Table 2. Process parameters.

Process Parameter	Value
Printing temperature	190 °C
Bed temperature	60 °C
Filling percentage	5%/25%/50%/75%
Layer height	0.2 mm
Material	Polylactic acid (PLA)

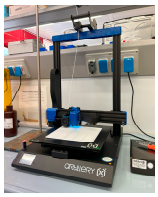

Below are the main features of the Sidewinder X2:

- Model: Artillery Sidewinder X2
- Build Volume: 300 × 300 × 400 mm
- Extruder Type: Direct Drive
- Auto-bed Leveling: Yes
- Heat Bed Type: AC heat bed
- Nozzle Type: Volcano
- Build Speed: 60 mm/s–150 mm/s
- Z-axis Design: Synchronized Dual Z System

This machine is equipped with a "Titan" extruder equipped with a "Volcano" nozzle that can reach a maximum extrusion temperature of 240 °C. A temperature of 190 °C isused to produce the specimens. The bed is heated with alternative current and can reach a temperature of 130 °C. In this study, a temperature of 60 °C was set to prevent the printed material from detaching from the printing bed.

Particularly, Figure 2a shows a Tri-Hexagon sample with an infill of 50% after production. The combination of triangles and hexagons can be seen. Figure 2b, on the other hand, shows the additive manufacturing process of the Gyroid sample with 50% infill. In this case, the core appears more complex, and the tridimensional structure can be seen.

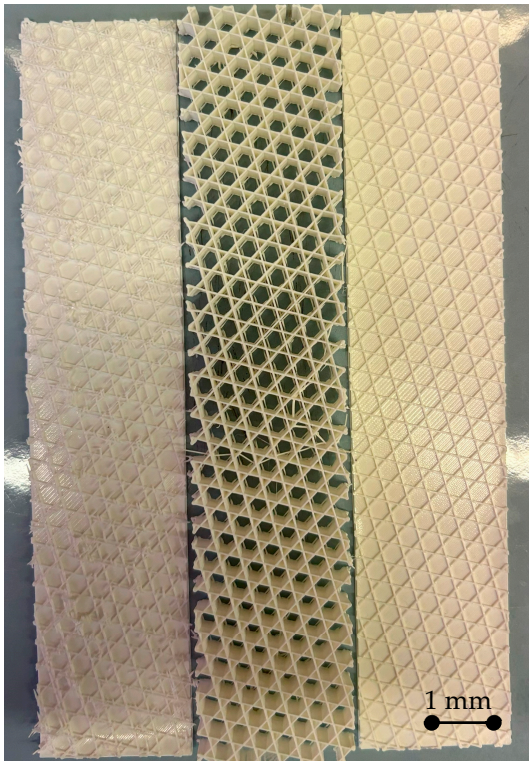

(**a**)

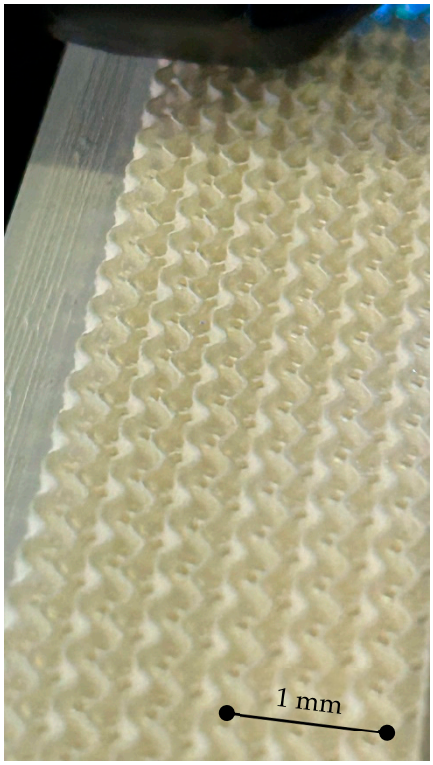

(**b**)

Figure 2. (**a**) Core of a Tri-Hexagon 50% sample after manufacturing process; (**b**) Additive manufacturing of a Gyroid 50% sample.

2.3. Flexural Tests

To carry out the mechanical characterization of the specimens, a "ZwichRoell" testing machine equipped with a 2.5 kN load cell was used, in accordance with ASTM D790 [62].

To carry out the bending tests, forty specimens were produced using AM, twenty of which had a Tri-Hexagon filling pattern and twenty with Gyroid geometry, i.e., five for each type. Each class of specimens, representing one of the two geometric patterns, was divided and then produced with four different filling densities, as previously mentioned. Five specimens were therefore produced for each filling density.

The tests were performed with a strain rate of 0.1 mm/min.

To analyze the samples and mainly to evaluate the failure modes, a Hirox Digital Microscope KH 8700 (Hirox, Tokyo, Japan) was used.

3. Results and Discussion

Figure 3 reports the typical load-displacement curves by varying the infill and the cell configuration (i.e., Tri-Hexagon and Gyroid). It is possible to observe that:

- For both the cell configurations, an infill equal to 5% leads to poor structural properties. In this case, the cell walls were unable to sustain the applied loads during flexural testing due to significant structural instability (Figure 4). In both types of structures, the thin-walled architecture lacks the necessary stiffness and strength at low density, making it highly susceptible to buckling under compressive stresses [63]. As the load increases, these thin walls initially deform elastically. However, due to their slenderness and geometric complexity, they rapidly reach a critical buckling threshold. Once this threshold is surpassed, the cell walls undergo localized collapse or crumpling, resulting in a significant reduction in load-bearing capacity and ultimately leading to structural failure. The unique geometries of both Tri-Hexagonal and Gyroid cells, while advantageous for weight reduction, limit their ability to evenly distribute and manage stresses, especially under bending loads. This makes them particularly prone to instability-related failures at low density. This phenomenon is illustrated in Figure 3, where the failure mode of a Tri-Hexagon 5% sample is reported.
- On increasing the infill, the load-displacement curve exhibits a characteristic response typical of higher-density sandwich structures under flexural testing [64]. At the beginning of the test, the load increases linearly with the displacement. This linear region indicates that the structure deforms elastically, which means that the material is returning to its original shape when the load is removed. The slope of this region reflects the stiffness of the structure, which is higher in this case due to the increased density of the material. As the load continues to increase, the curve reaches a peak value indicating the maximum load the structure can withstand before significant plastic deformation occurs. At this point, the cell walls of the structure begin to yield, and permanent deformation occurs. Following the peak load, cracks begin to form in the lower skin of the sandwich structure, particularly towards the point of contact with the punch, where the tensile stresses are highest (Figure 5). These tensile stresses cause micro-cracks to initiate, which subsequently propagate through the material. As these cracks grow, they lead to a reduction in the load-bearing capacity of the structure, which is reflected in the downward slope of the curve. The propagation of these cracks leads to a change in the slope of the load-displacement curve, indicating a loss of stiffness and the onset of material failure. As the cracks continue to grow and coalesce, the structure can no longer support the applied load, eventually leading to the failure of the sandwich panel. This phase is characterized by a gradual decrease in load, even if the displacement continues to increase. For higher-density Tri-Hexagon and Gyroid structures, the increased material density enhances the stiffness and strength, allowing the structure to withstand greater loads and exhibit more ductile behavior before failure. However, with continued loading, the tensile stresses in the lower skin lead to the formation and propagation of cracks, which ultimately govern the failure process. These cracks are a critical factor in the

observed change in slope and subsequent reduction in load-bearing capacity, leading to the eventual rupture of the structure.

- As the density of the Tri-Hexagon and Gyroid structures increases, the initial slope of the load-displacement curve becomes steeper, indicating an increase in stiffness. This is due to the reduction of voids within the structure as the density increases. With fewer voids, the material has a more continuous and solid network, allowing it to resist deformation more effectively under applied loads. This enhanced structural integrity requires a greater force to achieve the same displacement, reflecting the increased stiffness.
- The maximum load that the structures can withstand before they fail also increases with density, as indicated by the higher peak values in the load-displacement curves. The reduction in voids means that more material is available to distribute and bear the applied loads, leading to an enhanced load-bearing capacity. Denser structures are therefore able to sustain higher loads before significant plastic deformation and eventual failure occurs.

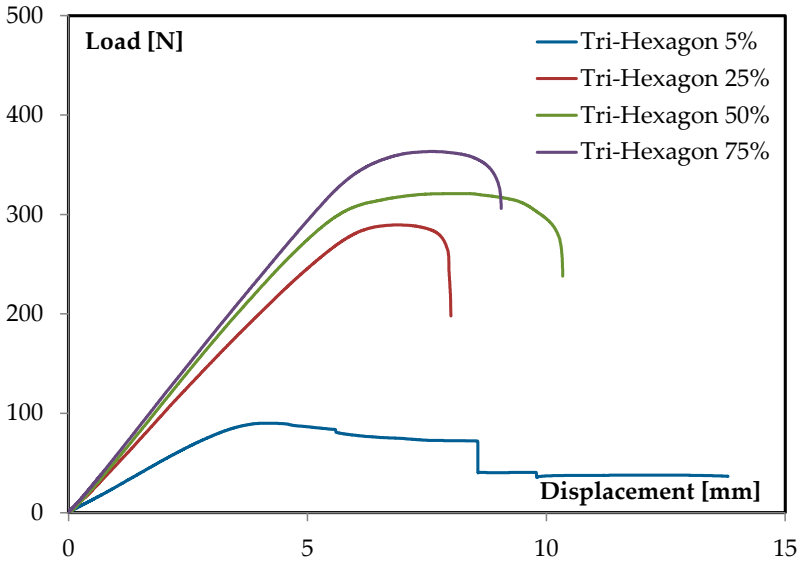

(**a**)

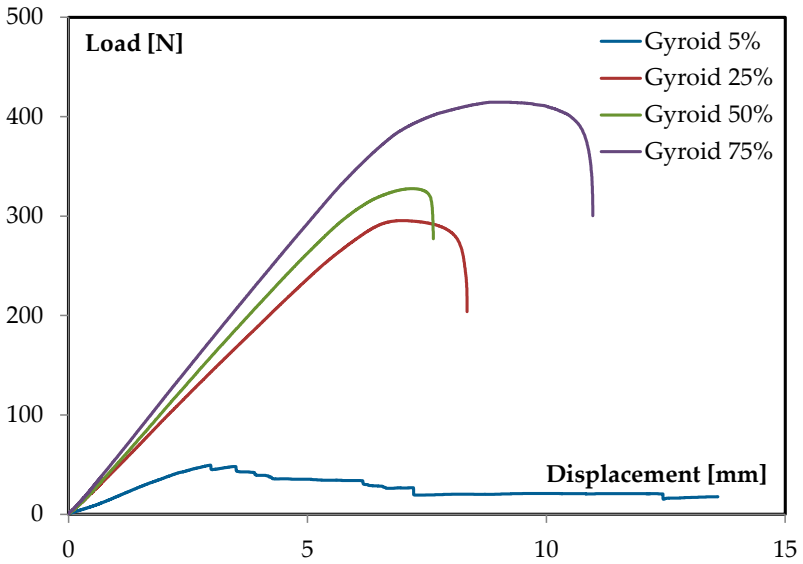

(**b**)

Figure 3. Typical load-displacement curves by varying the infill: (**a**) Tri-Hexagon; (**b**) Gyroid.

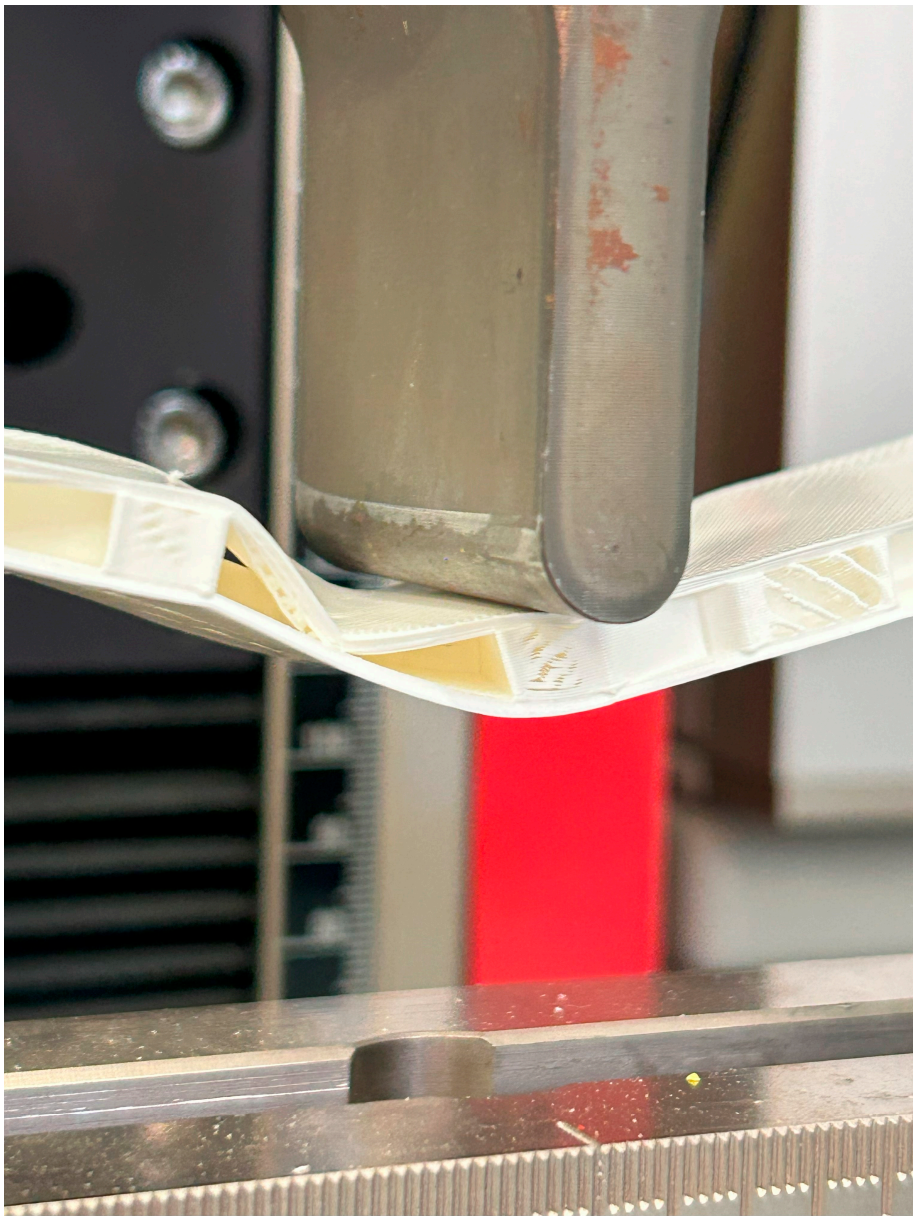

Figure 4. Failure mode of a Tri-Hexagon 5% structure.

The failure modes observed during flexural testing, as shown in Figures 4 and 5, reveal the structural response of the 3D-printed sandwich panels under load. In particular, the Tri-Hexagon structure (Figure 4) demonstrates buckling as the primary failure mode at low infill densities. This buckling occurs due to the collapse of the thin cell walls under compressive stress, highlighting the structural limitations when material distribution is insufficient. As the load increases, the lack of sufficient stiffness leads to significant deformation and eventual failure.

In Figure 5, which shows a Tri-Hexagon structure with higher infill, a different failure mechanism is observed. Here, the structure shows more ductile behavior, with cracks initiating in the lower skin and propagating through the core. This shift from buckling to crack propagation reflects the increased material density, which enhances the structure's ability to distribute loads more evenly. However, even with this improvement, the failure still originates at stress concentration points, such as the area near the punch in the three-point bending test. This analysis of failure modes during testing underscores the importance of balancing infill density and geometry to optimize structural performance under load.

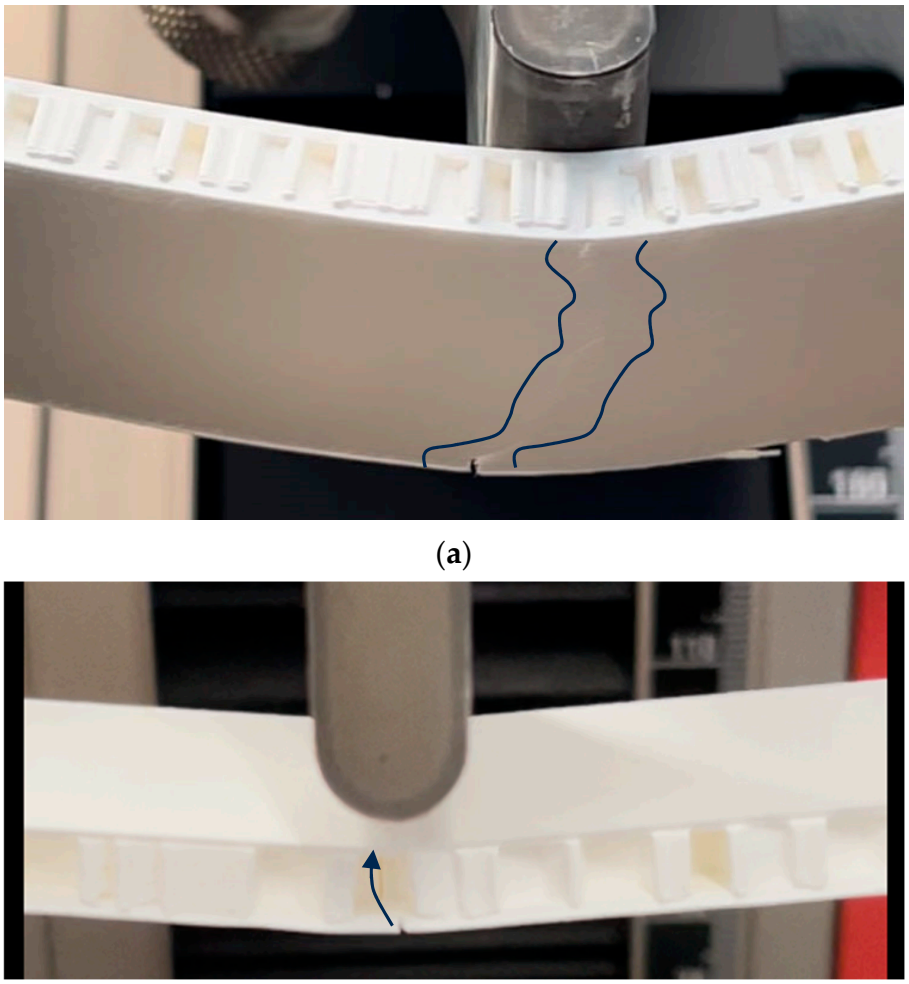

Figure 5. Failure mode of a Tri-Hexagon 50% structure: (**a**) cracks on the bottom skin; (**b**) propagation on the thickness.

Figure 6 compares the maximum loads by varying the infill and the cell configuration. The graph shows the following:

- At 5% density, the Tri-Hexagon structure exhibits a significantly higher maximum load compared to the Gyroid structure. This suggests that the Tri-Hexagon configuration has a better load-bearing capacity at lower densities, i.e., the 2D architecture allows for better resistance to the load. The standard deviation is also higher for the Tri-Hexagon structure, indicating greater variability in its performance. The Gyroid structure, while having a lower maximum load, shows less variability, which might imply more consistent performance but at a lower strength.
- At 25% density, the Gyroid structure surpasses the Tri-Hexagon in terms of maximum load capacity. This indicates that the Gyroid structure may have better strength or load distribution at this density. The standard deviation for the Gyroid is considerably lower, suggesting more uniform performance across all samples compared to the Tri-Hexagon. This could mean that the Gyroid structure is more reliable and consistent at this density, while the Tri-Hexagon has more variability in its load-bearing capacity.
- At 50% density, both structures show similar maximum load-bearing capacities, with the Tri-Hexagon slightly outperforming the Gyroid. The standard deviations at this density are relatively low for both, but the Tri-Hexagon has a slightly lower deviation, suggesting a slightly more consistent performance at this density. The similar

load capacities indicate that at mid-range density, both structures have comparable performance, but the Tri-Hexagon may offer a slight edge in terms of consistency.

- At 75% density, the Gyroid structure clearly outperforms the Tri-Hexagon in terms of maximum load capacity. This suggests that the Gyroid structure's design becomes more advantageous at higher densities, due to more effective load distribution and structural efficiency. The Gyroid also shows a much lower standard deviation, indicating a very consistent performance across all samples at this density. In contrast, the Tri-Hexagon structure, while still strong, shows slightly more variability in its performance.

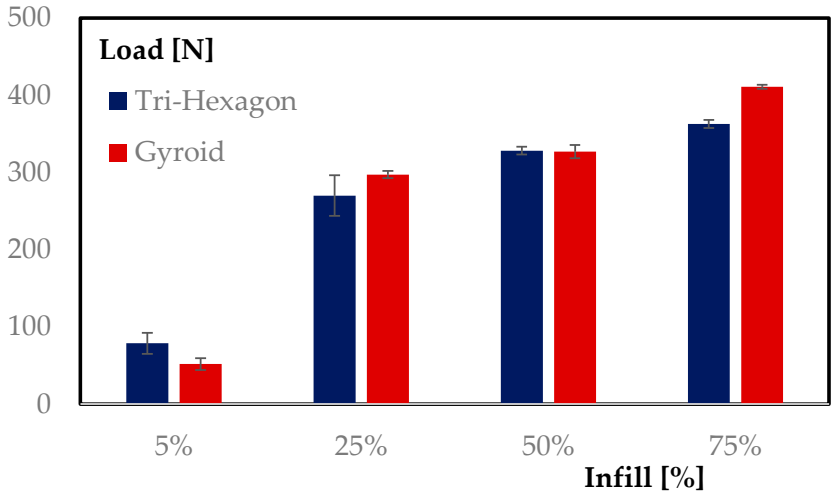

Figure 6. Comparison in maximum load between Tri-Hexagon and Gyroid structures.

To verify if the cell configuration is a significant parameter and, consequently, that it influences the flexural performance of the sample, a variance analysis was performed using MINITAB software 22.1.0, by considering the following factors:

- Cell configuration with 2 levels (i.e., Tri-Hexagon and Gyroid);
- Infill with 4 levels (i.e., 5%, 25%, 50%, and 75%).

In applying ANOVA, several assumptions were made, including the normality of residuals, homoscedasticity (equal variance), and independence of observations. These assumptions are fundamental to ensure that the ANOVA results are valid:

- Normality of residuals refers to the assumption that the differences between the observed and predicted values (i.e., residuals) follow a normal distribution. This ensures that the statistical tests used in ANOVA are appropriate for the data.
- Homoscedasticity (or equal variance) means that the variability in the response variable is consistent across all levels of the independent variables. This is important because unequal variances can lead to inaccurate estimates of the factor effects.
- Independence of observations implies that the data points are not related to each other. For example, the outcome of one observation should not influence another. Violations of this assumption can result in misleading conclusions.

To validate these assumptions, a detailed residual analysis was performed. As shown in Figure 7, the residuals are symmetrically distributed around zero, indicating normality. The assumption of homoscedasticity is confirmed by the consistent spread of residuals across the predicted values. No significant autocorrelation patterns were observed, affirming the independence of the data. These verifications indicate that the ANOVA results are reliable and that the significant effects observed are valid under the conditions of the study.

Table 3 summarizes the main results of the analysis of variance (ANOVA). The main objective was to determine whether the effects of the investigated factors on load were significant. DF are the degrees of freedom, used to calculate the mean square (MS).

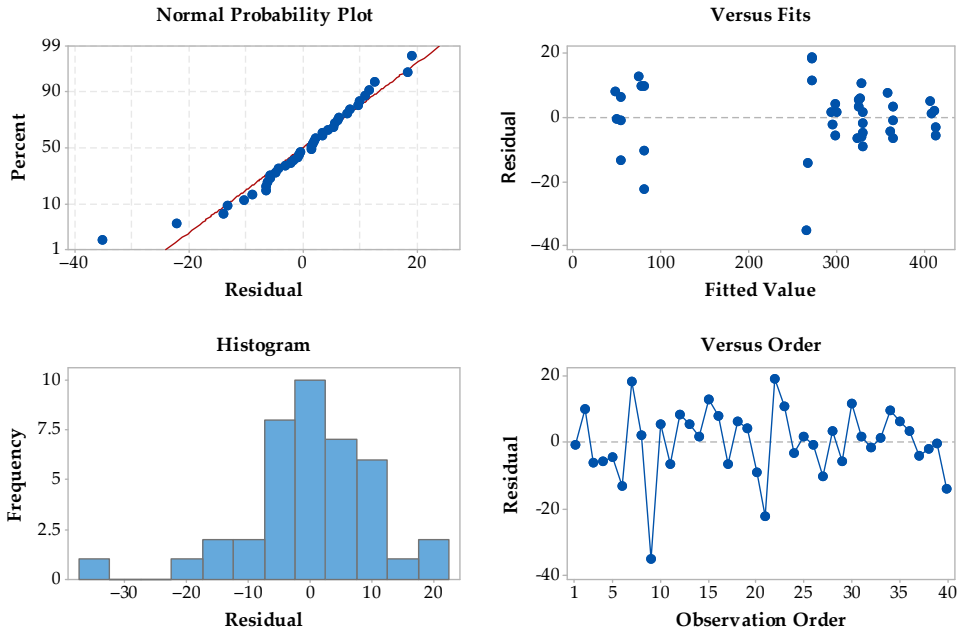

Figure 7. Residual plots for maximum load.

Table 3. ANOVA: Analysis of Variance for maximum load.

Source	DF	Adj SS	Adj MS	F-Value	*p*-Value
Model	11	599,647	54,513	367.46	0.000
Blocks	4	217	54	0.37	0.831
Linear	4	591,334	147,833	996.51	0.000
Cell	1	1418	1418	9.56	0.004
Infill	3	589,916	196,639	1325.50	0.000
2-Way Interactions	3	8097	2699	18,19	0.000
Cell*Infill	3	8097	2699	18,19	0.000
Error	28	4154	148		
Total	39	603,801			
S = 12.1799 | R-sq = 99.31% | R-sq(adj) = 99.04% | R-sq(pred) = 98.60%					

In general, they measure how much "independent" information is available to calculate each sum of squares (SS). This latter, also called the sum of the squared deviations, measures the total variability in the data, which is made up of: (i) the sum of squares for each of the two factors, which measures how much the means of the levels differ within each factor; (ii) the sum of squares for the interaction, which measures how much the effects of one factor depend on the level of the other factor; and (iii) the sum of squares for the error, which measures the variability that remains after the factors and the interaction have been taken into account. MS is simply the sum of squares (SS) divided by the degrees of freedom. The mean squared error is an estimate of the variance in the data that remains after accounting for the mean differences. F is used to determine the *p*-value (*p*), which defines whether the effect for a term is significant: i.e., if *p* is less than or equal to a selected level (e.g., 0.05), the effect for the term is significant.

From the table it is possible draw the following considerations:

- the individual effect of all the factors on the load is significant. The different infills induce a change in the level of maximum load that the sandwich can withstand, whereas the different cell structures induce different types of crack propagation, and consequently different behaviors depending on the kind infill by creating competition between the two cells.
- the interaction between the factors is also significant. This is evident in Figure 8, where the lines or intersects between them or are not parallel.

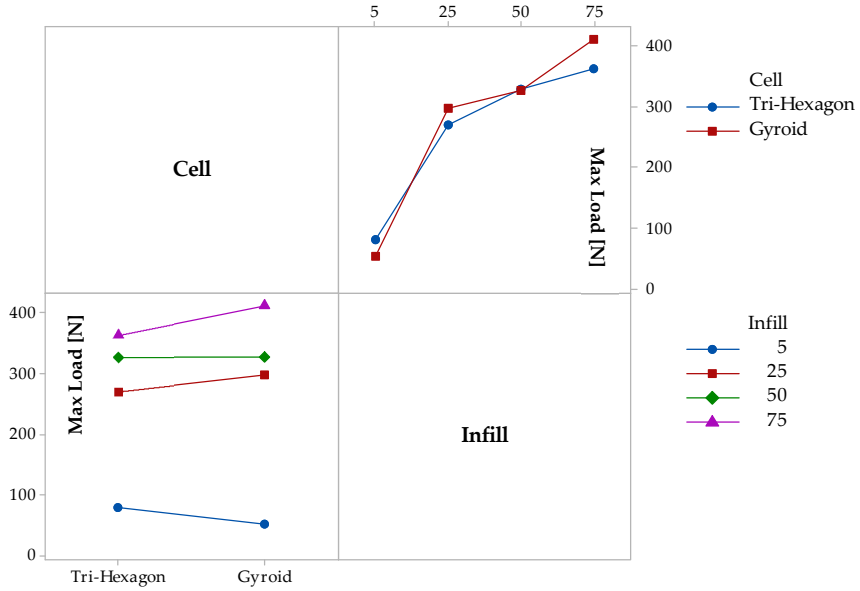

Figure 8. Interaction plot for maximum load.

Figure 9 summarizes the results for all the combinations investigated.

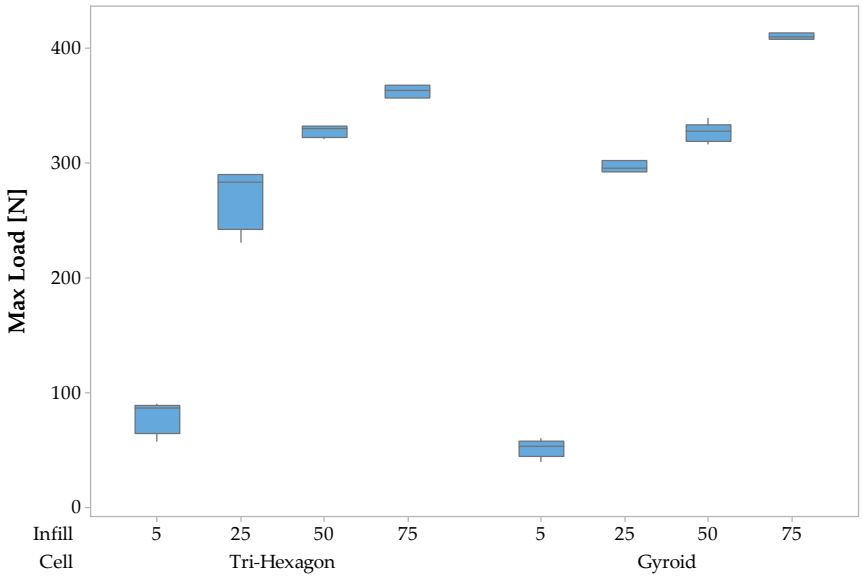

Figure 9. Interaction plot for maximum load.

While the statistical significance of factors such as core geometry and infill density is evident from the ANOVA, translating these findings into practical applications is crucial for advancing the field of additive manufacturing. In real-world applications, such as aerospace or automotive components, the trade-offs between mechanical performance and material efficiency become particularly important. The observed differences between geometries, where the Tri-Hexagon structure shows superior performance at lower densities, and the Gyroid structure, which excels at higher densities, suggest that the choice of structure should be application-specific. In situations where weight reduction is a priority, but mechanical integrity cannot be compromised, the Tri-Hexagon structure may be preferable at lower infills. Conversely, for applications requiring high structural efficiency, the Gyroid structure becomes more advantageous at higher infills. These trade-offs can guide the selection of the most appropriate configuration for specific needs, balancing factors such as material cost, production time, and mechanical performance.

Finally, optical microscope analysis shows the typical failure modes that occur in the two structures by varying the infill.

Figure 10 presents the analysis of a sample characterized by a Gyroid cell and an infill of 5%. For this structure, it is evident that the buckling phenomenon typical of the Try-Hexagon structure is coupled with an interlayer crack that affects the whole sample by causing its premature fracture. This phenomenon is due to the presence of several defects generated by the manufacturing process, the presence of which are promoted by the low infill. This explains the poorer behavior than with the Tri-Hexagon structure, where the 2D basis architecture involves only a fracture for buckling, as previously observed.

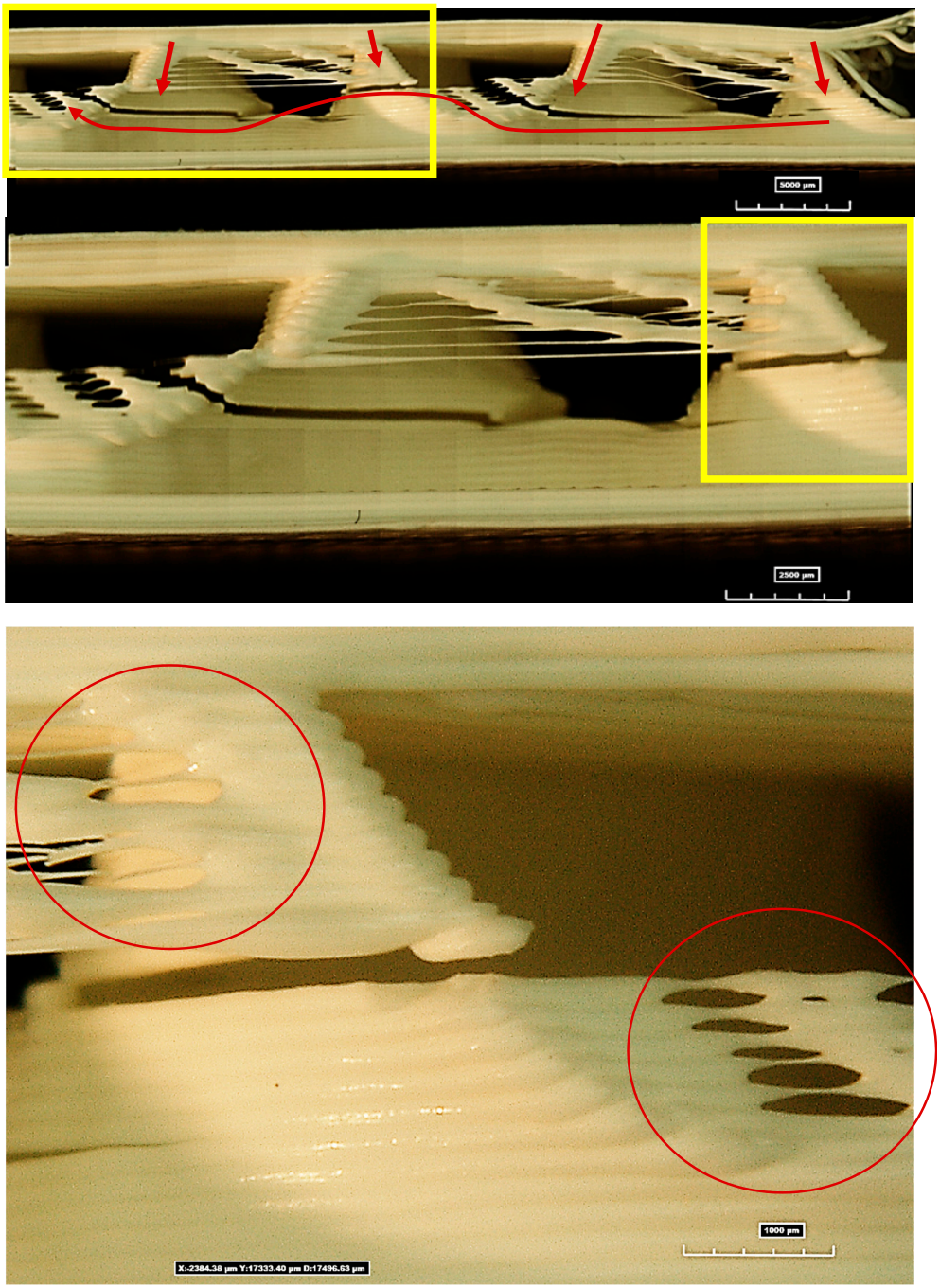

Figure 10. Optical analysis of a Gyroid 5% sample.

For higher infills, the structures of the samples are more compact and, consequently, these defects are not obvious. The crack starts in the lower skin near the pin, then it

propagates in the core and reaches the upper skin, leading to the failure of the sample, as can be observed in Figure 11 for a Gyroid 25% sample.

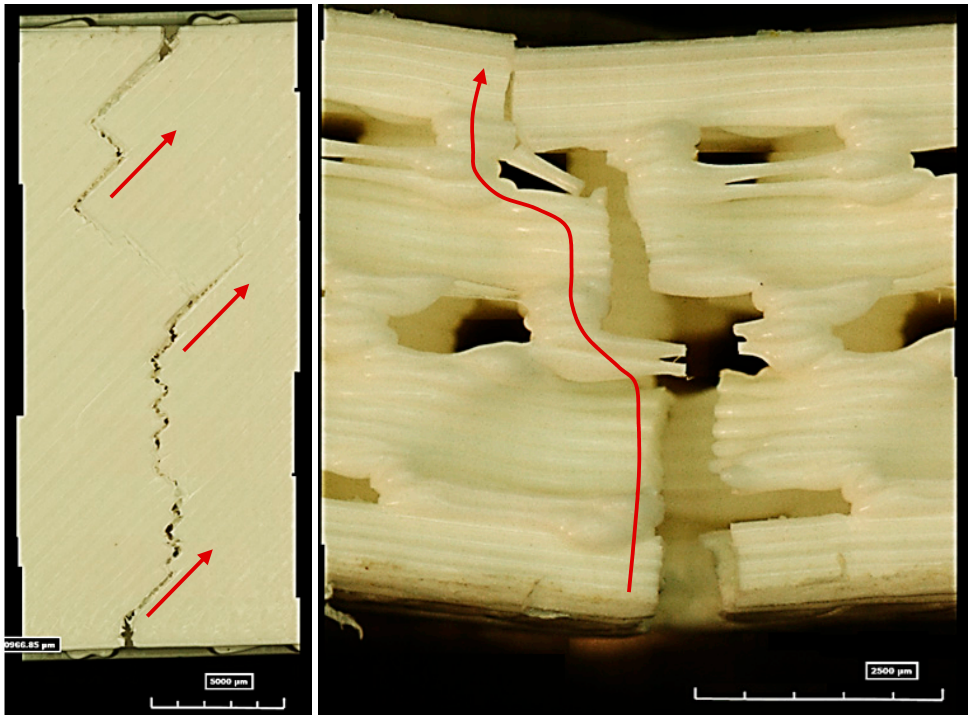

Figure 11. Optical analysis of a Gyroid 25% sample.

It is evident that:

- in the lower skin, the cracks mainly follow the direction of filament deposition;
- after the crack opens, this propagates into the core until it reaches the upper skin.

The detailed microscopy analysis presented in Figures 10 and 11 provides further insights into the failure mechanisms observed in the Gyroid structures at different infill densities. Figure 10 shows a Gyroid structure with 5% infill, where both buckling and interlayer cracking are evident. The presence of interlayer cracks suggests that the 3D printing process may have introduced defects, such as poor layer adhesion and voids, particularly at low infill levels. These defects, combined with the complex geometry of the Gyroid structure, lead to premature failure. The microscopy images highlight the limitations of current printing technology, and the challenges associated with achieving uniform material deposition, especially at low densities.

In contrast, Figure 11 illustrates the failure mode of a Gyroid structure with 25% infill. At this higher density, the structure exhibits a more compact and robust form, resulting in a different failure behavior. Here, the primary mode of failure is crack propagation, which begins in the lower skin and progresses through the core until it reaches the upper skin. This behavior is consistent with the findings from the flexural tests, where the increased material density leads to improved load distribution and a more ductile response. The direction of crack propagation aligns with the filament deposition pattern, indicating that even at higher densities, the printing process plays a crucial role in determining the failure characteristics of the structure. These observations emphasize the need for further optimization of both the printing process and the design of infill patterns to minimize defects and enhance the overall mechanical performance of 3D-printed sandwich structures.

The preferred direction of crack propagation that characterizes the Gyroid samples is not evident in the Tri-Hexagon sandwiches. Here, the crack follows a different trend corresponding to the cell walls and also after it has propagated into the core, as observed in Figure 12. This consideration explains the significance of the cell configuration.

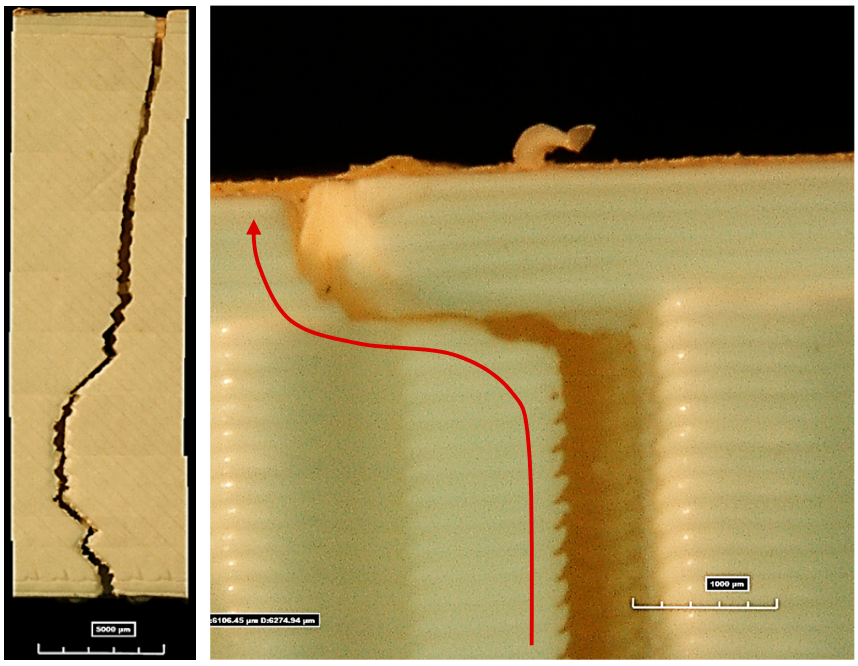

Figure 12. Optical analysis of a Tri-Hexagon 50% sample.

This optical analysis highlights the limitations of the technology used in this study. In fact, in addition to the defects generated by the low infill, the 3D printer caused both poor deposition of the filament, because the different layers are not perfectly distributed along the z-axis, and burning with a consequent deformation of the first layer, as can be seen in Figure 13 [65]. This can be overcome by using next-generation 3D printers, characterized by a closed chamber and a more rigid structure, as evidenced in Figure 14, where a sample of PLA, the subject of a future study, is realized by a Bambu Lab X1 Carbon.

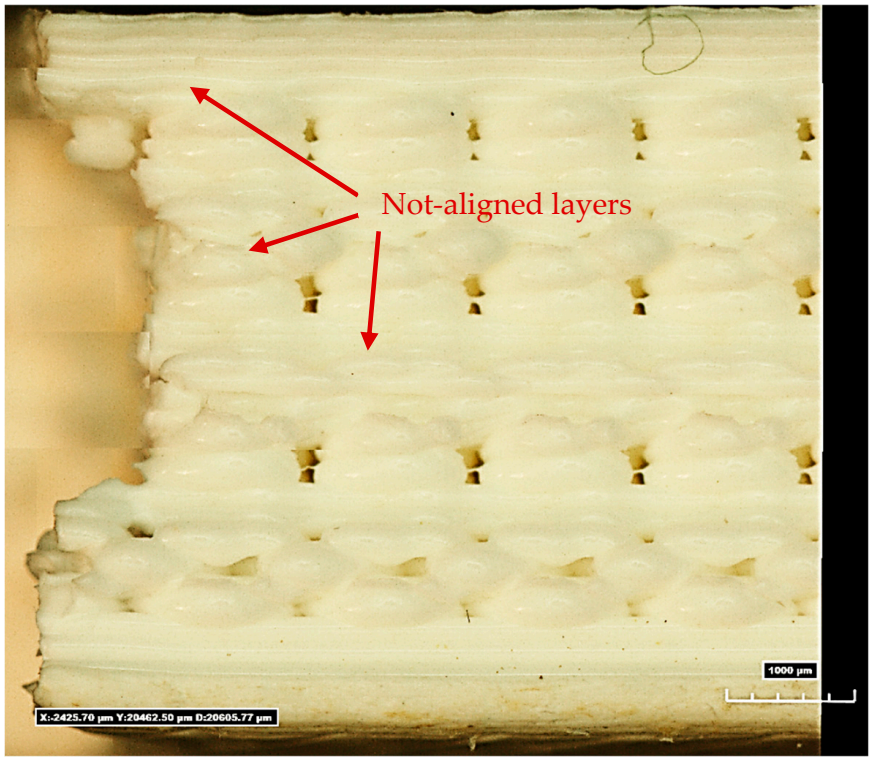

Figure 13. *Cont.*

Figure 13. Defects induced by technology.

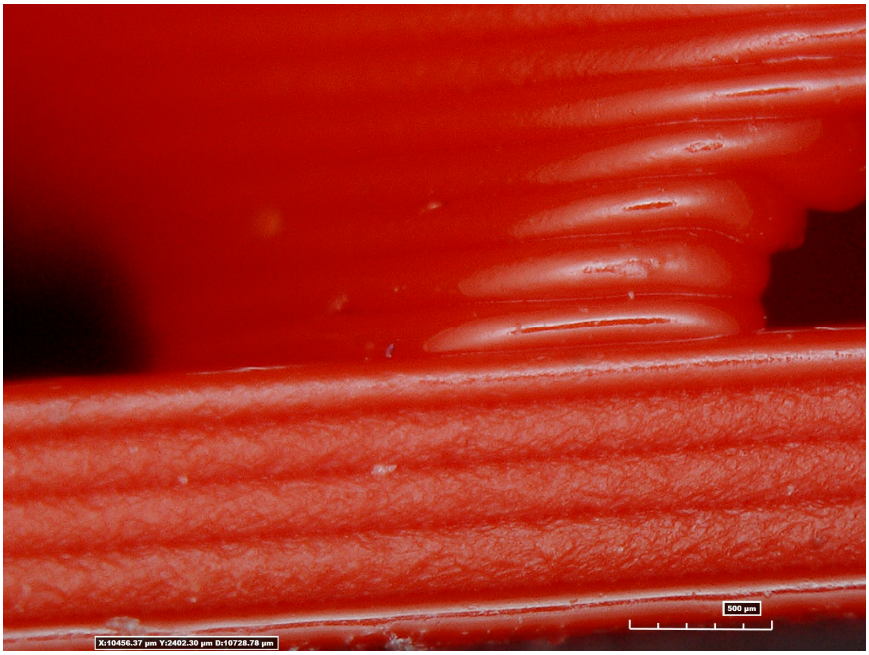

Figure 14. Example of sample in PLA generated on a next-generation 3D printer.

4. Conclusions

In this study, the additive manufacturing of PLA sandwich structures was optimized by varying the type of cell (i.e., the typical Tri-Hexagon and the new TPMS Gyroid) and infill (i.e., 5%, 25%, 50%, and 75%). The effects on flexural tests were investigated. It can be concluded that:

- For low infill (i.e., 5%), the architecture of the core for both cells does not resist, leading to premature failure. In the Tri-Hexagon samples, this occurs due to buckling, while in the Gyroid samples, buckling is coupled with interlayer fractures. This highlights the structural limitations of low-density infills, where the material distribution is insufficient to provide the necessary stiffness and load-bearing capacity.

- For high infill, the architectures are more resistant, and both cells exhibit good responses to bending loads. At these higher densities, cracks initiate at the lower skin and propagate through the core until reaching the upper skin. The difference between the two cells lies in the crack propagation direction: in Gyroid samples, the crack follows the direction of the filament deposition, while in the Tri-Hexagon samples, it follows the cell walls. This behavior underscores the importance of infill density in enhancing structural integrity, with both geometries showing improved performance as material density increases.

This behavior is confirmed by the analysis of variance (ANOVA), which demonstrates that both factors (i.e., cell geometry and infill) have a statistically significant impact on flexural behavior. For example, the Gyroid structure at 75% infill exhibited a maximum load-bearing capacity, outperforming the Tri-Hexagon structure. These findings suggest that, depending on the application, specific combinations of geometry and infill density can be tailored to optimize performance.

Moreover, the optical analysis reveals not only the differences in failure modes but also the defects introduced by the manufacturing process, such as unaligned layers, voids, and burns. These defects, particularly in low-density structures, further compromise mechanical performance.

Looking forward, future research should explore advanced printing technologies, such as multi-material printing or closed-chamber systems, to further minimize defects and improve the structural performance of 3D-printed sandwich structures. Additionally, expanding this research to other materials, including composites or polymers reinforced with fibers, could open new possibilities for developing high-performance structures with even greater versatility. By connecting these findings to the broader literature, ongoing advancements in additive manufacturing will continue to offer innovative solutions for complex engineering challenges.

Author Contributions: Conceptualization, G.D.B. and G.M.; methodology, G.D.B. and G.M.; software, G.M. and M.C.; validation, G.D.B., G.M. and M.C.; formal analysis, G.M. and M.C.; investigation, G.D.B., G.M. and M.C.; data curation, G.D.B., G.M. and M.C.; writing—original draft preparation, G.M.; writing—review and editing, G.D.B., G.M. and M.C.; supervision, G.D.B.; funding acquisition, G.D.B. All authors have read and agreed to the published version of the manuscript.

Funding: This research received no external funding.

Data Availability Statement: No new data were created or analyzed in this study. Data sharing is not applicable to this article.

Conflicts of Interest: The authors declare no conflicts of interest.

References

1. Ngo, T.D.; Kashani, A.; Imbalzano, G.; Nguyen, K.T.Q.; Hui, D. Additive Manufacturing (3D Printing): A Review of Materials, Methods, Applications and Challenges. *Compos. B Eng.* **2018**, *143*, 172–196. [CrossRef]
2. Shahrubudin, N.; Lee, T.C.; Ramlan, R. An Overview on 3D Printing Technology: Technological, Materials, and Applications. *Procedia Manuf.* **2019**, *35*, 1286–1296. [CrossRef]
3. DebRoy, T.; Wei, H.L.; Zuback, J.S.; Mukherjee, T.; Elmer, J.W.; Milewski, J.O.; Beese, A.M.; Wilson-Heid, A.; De, A.; Zhang, W. Additive Manufacturing of Metallic Components—Process, Structure and Properties. *Prog. Mater. Sci.* **2018**, *92*, 112–224. [CrossRef]
4. Tofail, S.A.M.; Koumoulos, E.P.; Bandyopadhyay, A.; Bose, S.; O'Donoghue, L.; Charitidis, C. Additive Manufacturing: Scientific and Technological Challenges, Market Uptake and Opportunities. *Mater. Today* **2018**, *21*, 22–37. [CrossRef]
5. Xu, F.; Liu, Z.; Selvaraj, R.; Ahsan, M. Bending and Eigenfrequency Analysis of Glass Fiber Reinforced Honeycomb Sandwich Shell Panels Containing Graphene-Decorated with Graphene Quantum Dots. *Eng. Struct.* **2023**, *294*, 116685. [CrossRef]
6. Birman, V.; Kardomateas, G.A. Review of Current Trends in Research and Applications of Sandwich Structures. *Compos. B Eng.* **2018**, *142*, 221–240. [CrossRef]
7. Moradi, A.; Ansari, R.; Hassanzadeh-Aghdam, M.K.; Jang, S.H. The Effect of Fuzzy Fiber-Reinforced Composite Skin on Bending Stiffness and Debonding Growth between Skin and Polymeric Foam Core of Sandwich Structures. *Eur. J. Mech. A/Solids* **2024**, *103*, 105182. [CrossRef]

8. Nian, Y.; Wan, S.; Li, X.; Su, Q.; Li, M. How Does Bio-Inspired Graded Honeycomb Filler Affect Energy Absorption Characteristics? *Thin-Walled Struct.* **2019**, *144*, 106269. [CrossRef]
9. Wang, H.; Chen, J.; Wang, C.; Guo, G.; An, Q.; Ming, W.; Chen, M. Burr Formation Mechanism and Morphological Transformation Critical Conditions in Grinding of Nickel-Based Superalloy Honeycomb Cores. *Chin. J. Aeronaut.* **2023**, *36*, 434–451. [CrossRef]
10. Chacón, J.M.; Caminero, M.A.; García-Plaza, E.; Núñez, P.J. Additive Manufacturing of PLA Structures Using Fused Deposition Modelling: Effect of Process Parameters on Mechanical Properties and Their Optimal Selection. *Mater. Des.* **2017**, *124*, 143–157. [CrossRef]
11. Ligon, S.C.; Liska, R.; Stampfl, J.; Gurr, M.; Mülhaupt, R. Polymers for 3D Printing and Customized Additive Manufacturing. *Chem. Rev.* **2017**, *117*, 10212–10290. [CrossRef] [PubMed]
12. Thomas, N.; Sreedhar, N.; Al-Ketan, O.; Rowshan, R.; Abu Al-Rub, R.K.; Arafat, H. 3D Printed Triply Periodic Minimal Surfaces as Spacers for Enhanced Heat and Mass Transfer in Membrane Distillation. *Desalination* **2018**, *443*, 256–271. [CrossRef]
13. Yuan, L.; Ding, S.; Wen, C. Additive Manufacturing Technology for Porous Metal Implant Applications and Triple Minimal Surface Structures: A Review. *Bioact. Mater.* **2019**, *4*, 56–70. [CrossRef] [PubMed]
14. Al-Ketan, O.; Abu Al-Rub, R.K. Multifunctional Mechanical Metamaterials Based on Triply Periodic Minimal Surface Lattices. *Adv. Eng. Mater.* **2019**, *21*, e56088. [CrossRef]
15. Al-Ketan, O.; Al-Rub, R.K.A.; Rowshan, R. Mechanical Properties of a New Type of Architected Interpenetrating Phase Composite Materials. *Adv. Mater. Technol.* **2017**, *2*, 1600235. [CrossRef]
16. Benedetti, M.; du Plessis, A.; Ritchie, R.O.; Dallago, M.; Razavi, N.; Berto, F. Architected Cellular Materials: A Review on Their Mechanical Properties towards Fatigue-Tolerant Design and Fabrication. *Mater. Sci. Eng. R Rep.* **2021**, *144*, 100606. [CrossRef]
17. Attarzadeh, R.; Rovira, M.; Duwig, C. Design Analysis of the "Schwartz D" Based Heat Exchanger: A Numerical Study. *Int. J. Heat. Mass. Transf.* **2021**, *177*, 121415. [CrossRef]
18. Krishnan, K.; Lee, D.-W.; Al Teneji, M.; Abu Al-Rub, R.K. Effective Stiffness, Strength, Buckling and Anisotropy of Foams Based on Nine Unique Triple Periodic Minimal Surfaces. *Int. J. Solids Struct.* **2022**, *238*, 111418. [CrossRef]
19. Iyer, J.; Moore, T.; Nguyen, D.; Roy, P.; Stolaroff, J. Heat Transfer and Pressure Drop Characteristics of Heat Exchangers Based on Triply Periodic Minimal and Periodic Nodal Surfaces. *Appl. Therm. Eng.* **2022**, *209*, 118192. [CrossRef]
20. Qureshi, Z.A.; Elnajjar, E.; Al-Ketan, O.; Al-Rub, R.A.; Al-Omari, S.B. Heat Transfer Performance of a Finned Metal Foam-Phase Change Material (FMF-PCM) System Incorporating Triply Periodic Minimal Surfaces (TPMS). *Int. J. Heat. Mass. Transf.* **2021**, *170*, 121001. [CrossRef]
21. Maskery, I.; Aremu, A.O.; Parry, L.; Wildman, R.D.; Tuck, C.J.; Ashcroft, I.A. Effective Design and Simulation of Surface-Based Lattice Structures Featuring Volume Fraction and Cell Type Grading. *Mater. Des.* **2018**, *155*, 220–232. [CrossRef]
22. Buchanan, C.; Gardner, L. Metal 3D Printing in Construction: A Review of Methods, Research, Applications, Opportunities and Challenges. *Eng. Struct.* **2019**, *180*, 332–348. [CrossRef]
23. Li, W.; Yu, G.; Yu, Z. Bioinspired Heat Exchangers Based on Triply Periodic Minimal Surfaces for Supercritical CO2 Cycles. *Appl. Therm. Eng.* **2020**, *179*, 115686. [CrossRef]
24. Attaran, M. The Rise of 3-D Printing: The Advantages of Additive Manufacturing over Traditional Manufacturing. *Bus. Horiz.* **2017**, *60*, 677–688. [CrossRef]
25. Li, T.; Wang, L. Bending Behavior of Sandwich Composite Structures with Tunable 3D-Printed Core Materials. *Compos. Struct.* **2017**, *175*, 46–57. [CrossRef]
26. Iranmanesh, N.; Yazdani Sarvestani, H.; Ashrafi, B.; Hojjati, M. Beyond Honeycombs: Core Topology's Role in 3D-Printed Sandwich Panels. *Mater. Today Commun.* **2023**, *37*, 107548. [CrossRef]
27. Wang, Y.; Liu, F.; Zhang, X.; Zhang, K.; Wang, X.; Gan, D.; Yang, B. Cell-Size Graded Sandwich Enhances Additive Manufacturing Fidelity and Energy Absorption. *Int. J. Mech. Sci.* **2021**, *211*, 106798. [CrossRef]
28. Lubombo, C.; Huneault, M.A. Effect of Infill Patterns on the Mechanical Performance of Lightweight 3D-Printed Cellular PLA Parts. *Mater. Today Commun.* **2018**, *17*, 214–228. [CrossRef]
29. Nian, Y.; Wan, S.; Avcar, M.; Yue, R.; Li, M. 3D Printing Functionally Graded Metamaterial Structure: Design, Fabrication, Reinforcement, Optimization. *Int. J. Mech. Sci.* **2023**, *258*, 108580. [CrossRef]
30. Sugiyama, K.; Matsuzaki, R.; Ueda, M.; Todoroki, A.; Hirano, Y. 3D Printing of Composite Sandwich Structures Using Continuous Carbon Fiber and Fiber Tension. *Compos. Part. A Appl. Sci. Manuf.* **2018**, *113*, 114–121. [CrossRef]
31. Nian, Y.; Wan, S.; Wang, X.; Zhou, P.; Avcar, M.; Li, M. Study on Crashworthiness of Nature-Inspired Functionally Graded Lattice Metamaterials for Bridge Pier Protection against Ship Collision. *Eng. Struct.* **2023**, *277*, 115404. [CrossRef]
32. Dilag, J.; Chen, T.; Li, S.; Bateman, S.A. Design and Direct Additive Manufacturing of Three-Dimensional Surface Micro-Structures Using Material Jetting Technologies. *Addit. Manuf.* **2019**, *27*, 167–174. [CrossRef]
33. Lee, J.Y.; An, J.; Chua, C.K. Fundamentals and Applications of 3D Printing for Novel Materials. *Appl. Mater. Today* **2017**, *7*, 120–133. [CrossRef]
34. Dizon, J.R.C.; Espera, A.H.; Chen, Q.; Advincula, R.C. Mechanical Characterization of 3D-Printed Polymers. *Addit. Manuf.* **2018**, *20*, 44–67. [CrossRef]
35. Wang, X.; Jiang, M.; Zhou, Z.; Gou, J.; Hui, D. 3D Printing of Polymer Matrix Composites: A Review and Prospective. *Compos. B Eng.* **2017**, *110*, 442–458. [CrossRef]
36. Guo, H.; Lv, R.; Bai, S. Recent Advances on 3D Printing Graphene-Based Composites. *Nano Mater. Sci.* **2019**, *1*, 101–115. [CrossRef]

37. Marabello, G.; Borsellino, C.; Di Bella, G. Carbon Fiber 3D Printing: Technologies and Performance—A Brief Review. *Materials* **2023**, *16*, 7311. [CrossRef] [PubMed]
38. Wang, Z.; Yao, G. Nonlinear Vibration and Stability of Sandwich Functionally Graded Porous Plates Reinforced with Graphene Platelets in Subsonic Flow on Elastic Foundation. *Thin-Walled Struct.* **2024**, *194*, 111327. [CrossRef]
39. Sukia, I.; Morales, U.; Esnaola, A.; Aurrekoetxea, J.; Erice, B. Low-Velocity Impact Performance of Integrally-3D Printed Continuous Carbon Fibre Composite Sandwich Panels. *Mater. Lett.* **2024**, *354*, 135374. [CrossRef]
40. Penumakala, P.K.; Santo, J.; Thomas, A. A Critical Review on the Fused Deposition Modeling of Thermoplastic Polymer Composites. *Compos. B Eng.* **2020**, *201*, 108336. [CrossRef]
41. Ayrilmis, N. Effect of Layer Thickness on Surface Properties of 3D Printed Materials Produced from Wood Flour/PLA Filament. *Polym. Test.* **2018**, *71*, 163–166. [CrossRef]
42. Peng, X.; Zhang, M.; Guo, Z.; Sang, L.; Hou, W. Investigation of Processing Parameters on Tensile Performance for FDM-Printed Carbon Fiber Reinforced Polyamide 6 Composites. *Compos. Commun.* **2020**, *22*, 100478. [CrossRef]
43. Yao, T.; Deng, Z.; Zhang, K.; Li, S. A Method to Predict the Ultimate Tensile Strength of 3D Printing Polylactic Acid (PLA) Materials with Different Printing Orientations. *Compos. B Eng.* **2019**, *163*, 393–402. [CrossRef]
44. Feng, J.; Liu, B.; Lin, Z.; Fu, J. Isotropic Porous Structure Design Methods Based on Triply Periodic Minimal Surfaces. *Mater. Des.* **2021**, *210*, 110050. [CrossRef]
45. Jones, A.; Leary, M.; Bateman, S.; Easton, M. TPMS Designer: A Tool for Generating and Analyzing Triply Periodic Minimal Surfaces[Formula Presented]. *Softw. Impacts* **2021**, *10*, 100167. [CrossRef]
46. Feng, J.; Fu, J.; Yao, X.; He, Y. Triply Periodic Minimal Surface (TPMS) Porous Structures: From Multi-Scale Design, Precise Additive Manufacturing to Multidisciplinary Applications. *Int. J. Extrem. Manuf.* **2022**, *4*, 022001. [CrossRef]
47. Dixit, T.; Al-Hajri, E.; Paul, M.C.; Nithiarasu, P.; Kumar, S. High Performance, Microarchitected, Compact Heat Exchanger Enabled by 3D Printing. *Appl. Therm. Eng.* **2022**, *210*, 118339. [CrossRef]
48. Qureshi, Z.A.; Al-Omari, S.A.B.; Elnajjar, E.; Al-Ketan, O.; Al-Rub, R.A. Using Triply Periodic Minimal Surfaces (TPMS)-Based Metal Foams Structures as Skeleton for Metal-Foam-PCM Composites for Thermal Energy Storage and Energy Management Applications. *Int. Commun. Heat. Mass. Transf.* **2021**, *124*, 105265. [CrossRef]
49. Attarzadeh, R.; Attarzadeh-Niaki, S.H.; Duwig, C. Multi-Objective Optimization of TPMS-Based Heat Exchangers for Low-Temperature Waste Heat Recovery. *Appl. Therm. Eng.* **2022**, *212*, 118448. [CrossRef]
50. Qureshi, Z.A.; Al-Omari, S.A.B.; Elnajjar, E.; Al-Ketan, O.; Abu Al-Rub, R. Nature-Inspired Triply Periodic Minimal Surface-Based Structures in Sheet and Solid Configurations for Performance Enhancement of a Low-Thermal-Conductivity Phase-Change Material for Latent-Heat Thermal-Energy-Storage Applications. *Int. J. Therm. Sci.* **2022**, *173*, 107361. [CrossRef]
51. Nian, Y.; Wan, S.; Zhou, P.; Wang, X.; Santiago, R.; Li, M. Energy Absorption Characteristics of Functionally Graded Polymer-Based Lattice Structures Filled Aluminum Tubes under Transverse Impact Loading. *Mater. Des.* **2021**, *209*, 110011. [CrossRef]
52. Xie, C.; Wang, D.; Zong, L.; Kong, D. Crashworthiness Analysis and Multi-Objective Optimization of Spatial Lattice Structure under Dynamic Compression. *Int. J. Impact Eng.* **2023**, *180*, 104713. [CrossRef]
53. Clarke, D.A.; Dolamore, F.; Fee, C.J.; Galvosas, P.; Holland, D.J. Investigation of Flow through Triply Periodic Minimal Surface-Structured Porous Media Using MRI and CFD. *Chem. Eng. Sci.* **2021**, *231*, 116264. [CrossRef]
54. Qureshi, Z.A.; Al Omari, S.A.B.; Elnajjar, E.; Mahmoud, F.; Al-Ketan, O.; Al-Rub, R.A. Thermal Characterization of 3D-Printed Lattices Based on Triply Periodic Minimal Surfaces Embedded with Organic Phase Change Material. *Case Stud. Therm. Eng.* **2021**, *27*, 101315. [CrossRef]
55. Mirabolghasemi, A.; Akbarzadeh, A.H.; Rodrigue, D.; Therriault, D. Thermal Conductivity of Architected Cellular Metamaterials. *Acta Mater.* **2019**, *174*, 61–80. [CrossRef]
56. Qureshi, Z.A.; Addin Burhan Al-Omari, S.; Elnajjar, E.; Al-Ketan, O.; Al-Rub, R.A. On the Effect of Porosity and Functional Grading of 3D Printable Triply Periodic Minimal Surface (TPMS) Based Architected Lattices Embedded with a Phase Change Material. *Int. J. Heat. Mass. Transf.* **2022**, *183*, 122111. [CrossRef]
57. Lu, Y.; Zhao, W.; Cui, Z.; Zhu, H.; Wu, C. The Anisotropic Elastic Behavior of the Widely-Used Triply-Periodic Minimal Surface Based Scaffolds. *J. Mech. Behav. Biomed. Mater.* **2019**, *99*, 56–65. [CrossRef]
58. Dudescu, C.; Racz, L. Effects of Raster Orientation, Infill Rate and Infill Pattern on the Mechanical Properties of 3D Printed Materials. *ACTA Univ. Cibiniensis* **2017**, *69*, 23–30. [CrossRef]
59. Shanmugam, V.; Das, O.; Babu, K.; Marimuthu, U.; Veerasimman, A.; Johnson, D.J.; Neisiany, R.E.; Hedenqvist, M.S.; Ramakrishna, S.; Berto, F. Fatigue Behaviour of FDM-3D Printed Polymers, Polymeric Composites and Architected Cellular Materials. *Int. J. Fatigue* **2021**, *143*, 106007. [CrossRef]
60. Singh, S.; Singh, G.; Prakash, C.; Ramakrishna, S. Current Status and Future Directions of Fused Filament Fabrication. *J. Manuf. Process* **2020**, *55*, 288–306. [CrossRef]
61. Popescu, D.; Zapciu, A.; Amza, C.; Baciu, F.; Marinescu, R. FDM Process Parameters Influence over the Mechanical Properties of Polymer Specimens: A Review. *Polym. Test.* **2018**, *69*, 157–166. [CrossRef]
62. *ASTM D790-17*; Standard Test Methods for Flexural Properties of Unreinforced and Reinforced Plastics and Electrical Insulating Materials. ASTM International: West Conshohocken, PA, USA, 2017.
63. Daynes, S. High Stiffness Topology Optimised Lattice Structures with Increased Toughness by Porosity Constraints. *Mater. Des.* **2023**, *232*, 112183. [CrossRef]

64. Epasto, G.; Rizzo, D.; Landolfi, L.; Detry, A.L.H.S.; Papa, I.; Squillace, A. Design of Monomaterial Sandwich Structures Made with Foam Additive Manufacturing. *J. Manuf. Process* **2024**, *121*, 323–332. [CrossRef]
65. Kim, S.; Kim, E.-H.; Lee, W.; Sim, M.; Kim, I.; Noh, J.; Kim, J.-H.; Lee, S.; Park, I.; Su, P.-C.; et al. Real-Time in-Process Control Methods of Process Parameters for Additive Manufacturing. *J. Manuf. Syst.* **2024**, *74*, 1067–1090. [CrossRef]